PERFORMANCE ANALYSIS OF EBS-CCD IMAGING TUBES/STATUS OF ICCD DEVELOPMENT*

J. B. Barton
Texas Instruments Incorporated
Dallas, Texas

J. J. Cuny
ITT Electro-Optical Products Division
Fort Wayne, Indiana

D. R. Collins
Texas Instruments Incorporated
Dallas, Texas

ABSTRACT. The low-light-level imaging performance of different EBS-CCD tubes are analytically compared, along with that predicted for direct-view CCD imagers, using the psychophysical model of Rosell and Willson. Because its primary photosurface is silicon, the quantum efficiency of the direct-view CCD is higher than that of the EBS-CCD. However, since there is no gain prior to CCD readout, the noise-equivalent signal is considerably higher for the direct-view CCD, even when it is assumed that the noise is dominated by amplifier noise of a few tens of electrons per packet. For this assumption to be valid, the CCD must be cooled below room temperature in some fashion. Thus, in comparison with other forms of low-light-level image sensors, the EBS-CCD tube appears to offer significant advantages in terms of size, sensitivity, and temperature of operation. The second part of this paper briefly outlines the primary objectives of the current intensified CCD programs being pursued jointly by Texas Instruments and the ITT Electro-Optical Products Division. A discussion is given of the compatibility problems associated with subjecting a CCD array to the effects of vacuum tube processing. The two CCD tube designs being developed are described, and results are presented based on current data available.

I. PERFORMANCE ANALYSIS OF EBS-CCD IMAGING TUBES

A. PSYCHOPHYSICAL MODEL

The psychophysical model used in the analysis of low-light level television (LLLTV) imager performance presented in this paper is based on the model developed by Rosell and Willson[1] for conventional imaging tubes. Through an extensive series of psychophysical experiments with observers watching TV displays of selected imagery, these two researchers have verified that the limiting resolution to which an observer can perceive a bar pattern is proportional to the display signal-to-noise ratio, over a wide range of conditions. Rosell and Willson define the display signal-to-noise ratio ρ_D, for imaging a dark and light bar pattern as follows:

$$\rho_D(f) = \frac{R_t^{SF}(f)\, C_M\, 2\, N_{av}}{B\left[\left(N_{av} + N_{ns}^2\right)^{1/2}\right]}, \qquad (1)$$

where $R_t^{SF}(f)$ = total square-wave flux response of the system at the bar pattern spatial frequency, f,

$$= \frac{8}{\pi^2}\left|\sum_{n=1,3,5,\ldots} \frac{1}{n^2} R_t(nf)\right| ;$$

$R_t(f)$ = total modulation transfer function (MTF) of the system at spatial frequency, f;

C_M = modulation contrast of the bar pattern focused onto the sensor

$$= \frac{H_{max} - H_{min}}{H_{max} + H_{min}} ;$$

H_{max} = maximum sensor irradiance;

H_{min} = minimum sensor irradiance;

*This work supported in part by the U. S. Navy (NAVELEX Contract No. N00039-73-C-0070) and the U. S. Army (NVL Contracts No. DAAK02-73-C-0195 and DAAK02-74-C-0359).

N_{av} = average number of signal photoelectrons actually generated within the image of a bar during τ_{eye}, averaged over a bar pair, where τ_{eye} is the integration time of the eye (Rosell and Willson use 0.1 second for τ_{eye})

= N_{np}^2, where N_{np} is the rms noise on the Poisson process of generating photoelectrons at the primary photosurface (photon noise);

N_{ns} = equivalent rms number of noise electrons per bar added to the video signal by other noise sources in the system; and

B = operator which represents noise reduction by system MTF effects.

With this definition of ρ_D, Rosell and Willson have shown that a bar pattern imaged by a sensor can just be resolved by an observer viewing the output of the sensor on a display when ρ_D for that pattern and sensor combination is equal to about 2.5. The observer is allowed to optimally adjust the display contrast and brightness and his own viewing distance. This threshold value, ρ_{th}, for ρ_D is not absolutely constant, but varies somewhat as the bar length-to-width ratio, r_{LW}, is changed, with a somewhat larger value of ρ_{th} required for larger values of r_{LW} ($\leq$25% increase as r_{LW} is varied from 5 to 20). ρ_{th} also depends on f, the spatial frequency of the pattern, being slightly smaller for the higher frequencies ($\approx$ 25% decrease as f varies from 100 to 500 TV lines per picture height, for r_{LW} = 5). In the present treatment, the somewhat conservative value of 3.0 has been used for ρ_{th} throughout, regardless of the values of r_{LW} and f.

There are noise sources in a CCD that insert a fixed system noise component into each picture element once each frame, or once each field in the case of interlaced operation. An example of this type of noise is the preset noise introduced at the CCD output by a simple precharge amplifier. The time averaged value of this noise, averaged over τ_{eye}, thus depends on the frame rate. For the CCD, therefore, it is preferable to redefine N_{av} and N_{ns} as averages over τ_f, a single frame time, or field time for interlaced mode, and to account for the eye's integration time through a separate factor,

$$\sqrt{\tau_{eye}/\tau_f} \ .$$

Equation (1) then becomes:

$$\rho_D(f) = \frac{R_t^{SF}(f)\ C_M\ 2\ N_{av}\sqrt{\tau_{eye}/\tau_f}}{B\left[(N_{av} + N_{ns}^2)^{1/2}\right]} \ . \qquad (2)$$

This use of the eye integration factor is justified only if the noise is uncorrelated from one frame to the next, but this will, in general, be true. The only exception is so-called "fixed pattern noise," resulting from fixed spatial variations in the sensor background level or responsivity. The amplitudes of these variations add directly, rather than in quadrature. If N_{nf} is the equivalent rms number of fixed pattern noise electrons per bar image, averaged over a bar pair and integrated over τ_f, the appropriate modification of Equation (2) to include fixed pattern noise is

$$\rho_D(f) = \frac{R_t^{SF}(f)\ C_M\ 2\ N_{av}}{B\left\{\left[(N_{av}+N_{ns}^2)(\tau_f/\tau_{eye}) + N_{nf}^2\right]\right\}^{1/2}} \ . (3)$$

This treatment of fixed pattern noise represents an extension beyond the work of Rosell and Willson, and is consequently somewhat speculative. For this reason, fixed pattern noise is ignored in most of the computer predictions of limiting resolution presented here. However, the arguments seem plausible enough to justify a plot that includes an estimate of fixed pattern noise.

In applying the results of Rosell and Willson to CCD's, it is more convenient to express the signal and noise in terms of electrons per picture element, or pixel, rather than per bar. If we assume for the moment that system MTF effects are negligible and that all noise sources are white, we can write Equation (3) as

$$\rho_D(f) = \frac{R_t^{SF}(f)\ C_M\ 2\ mn\ N'_{av}}{\left\{(N'_{av}\ mn + N'^2_{ns}\ mn)(\tau_f/\tau_{eye}) + N'^2_{nf} mn\right\}^{1/2}}$$

$$= \frac{2\ R_t^{SF}(f)\ C_M\ N'_{av}}{\left\{\left[(N'_{av} + N'^2_{ns})(\tau_f/\tau_{eye}) + N'^2_{nf}\right]/mn\right\}^{1/2}}, \ (4)$$

where N'_{av} = average number of signal photoelectrons collected per pixel during τ_f, averaged over a bar pair;

N'_{ns} = equivalent rms number of system noise electrons per pixel per frame (or field), averaged over a bar pair;

N'_{nf} = equivalent rms number of fixed pattern noise electrons per pixel per frame (or field), averaged over a bar pair;

m = number of pixels per bar height; and

n = number of pixels per bar width.

The reduction in noise power by the divisor, mn, may be interpreted as bandlimiting by the eye as it integrates over a bar. Elaborating on this interpretation, we set

$S_p(f_x,f_y)$ = spectral density of average photon noise per pixel,

$S_s(f_x,f_y)$ = spectral density of system noise per pixel, and

$S_f(f_x,f_y)$ = spectral density of fixed pattern noise per pixel, where f_x, f_y are frequencies in the two-dimensional transform space of the two-dimensional sensor surface.

Then $$\frac{N'^2_{av} + N'^2_{ns}\left(\frac{\tau_f}{\tau_{eye}}\right) + N'^2_{nf}}{mn}$$

$$= \int_0^{f_{Nx}/n} df_x \int_0^{f_{Ny}/m} df_y \left\{\left[S_p(f_x,f_y) + S_s(f_x,f_y)\right] \times (\tau_f/\tau_{eye}) + S_f(f_x,f_y)\right\} , \quad (5)$$

where f_{Nx} = Nyquist frequency in the x-direction,

f_{Ny} = Nyquist frequency in the y-direction.

Substituting Equation (5) into Equation (4) yields

$$\rho_D(f) = \frac{2\, R_t^{SF}(f)\, C_M\, N'_{av}}{\left(\int_0^{f_{Nx}/n} df_x \int_0^{f_{Ny}/m} df_y \left\{\left[S_p(f_x, f_y) + S_s(f_x, f_y)\right]\left(\frac{\tau_f}{\tau_{eye}}\right) + S_f(f_x, f_y)\right\}\right)^{1/2}} \quad (6)$$

If the spectral densities in Equation (6) are interpreted as representing noise referred to the CCD output channel, then this expression for ρ_D is general enough to include non-white noise sources and subunity MTF's.

The bandlimiting of noise spectral sity is explicitly represented in Equation (6) by the integration limits in the denominator, with a maximum noise bandwidth equal to the maximum signal bandwidth (Nyquist frequency). The divisors, n and m, are functions of f, through the relationships:

$$\text{Vertical Bars} \begin{cases} n = f_{Nx}/f, \\ m = nr_{LW}, \end{cases}$$

$$\text{Horizontal Bars} \begin{cases} m = f_{Ny}/f, \\ n = mr_{LW}. \end{cases}$$

In the graphical presentation of computational results that follow, the spatial frequencies are expressed in TV lines per picture height (TVL/PH). The presentation in terms of TVL/PH is consistent with Rosell and Willson's graphical format and is of more direct utility to the display observer than a presentation in terms of line pairs per millimeter (ℓp/mm), since it includes information concerning sensor size in addition to sensor resolution density.

In order to use Equation (6) to compute ρ_D, expressions were developed for $R_t^{SF}(f)$, $S_p(f_x,f_y)$ and $S_s(f_x, f_y)$ in terms of predictable system parameters. For the present computations, the MTF factors that were used to calculate $R_t^{SF}(f)$ were the following:

(1) Diffusion MTF;
(2) Secondary generation MTF (for EBS-CCD only);
(3) Pixel collection MTF;
(4) Charge transfer MTF;
(5) Lens MTF;
(6) Tube pretarget MTF (for EBS-CCD only).

The noise components that were considered in calculating $S_s(f_x, f_y)$ were the following: (1) Dark current noise, and (2) Amplifier noise.

Fat zero input noise and fast interface state noise were not included, as the sensors were assumed to be buried channel. Bulk state trapping noise was not included, as measurement data on this noise source are somewhat sparse. The expressions developed for these various MTF's and noise spectral densities are too detailed to be presented here, but are contained in a report to NVL.[2]

B. COMPUTER PREDICTIONS OF LIMITING RESOLUTION

Five different types of CCD imagers were analyzed by computer using the display signal-to-noise ratio model described in the preceding section to predict limiting resolution versus illumination level. More precisely, five different applications of the same CCD array in image sensor configurations were analyzed:

(1) Direct-view CCD sensor, cooled to T = 210 K, with responsivity of 90 mA/W for 2854 K illumination = 5.6 mA/ℓm;

(2) Proximity-focused EBS-CCD tube, operating at T = 300 K, with S-20 extended red response photocathode (responsivity of 7 mA/W for 2854 K illumination = 440 μA/ℓm);

(3) Proximity-focused EBS-CCD tube, at T = 300 K, with GaAs photocathode (responsivity of 6.4 mA/W for 2854 K illumination = 390 μA/ℓm);

(4) EBS-CCD inverter tube, at T = 300 K, with 25 mm S-20 extended red response photocathode;

(5) EBS-CCD inverter tube, at T = 300 K, with 25 mm GaAs photocathode.

The CCD array assumed for each of these applications is a thinned, rear-illuminated (or bombarded), 500 x 500-element CCD with a 3:4 aspect ratio, operated in the frame transfer mode with 2:1 interlace (resulting in a possible 500 displayed TV lines). The pixel dimensions are assumed to be 0.9 mil by 1.35 mil, resulting in an active sensor diagonal of 14.3 mm.

These five configurations are compared in a series of plots of limiting resolution, evaluated at the center of the active sensor, versus average sensor irradiance in Figures 1 through 5, where each plot represents a different set of operating conditions. The first case analyzed is the photon-noise-limited resolution of 50% contrast vertical bars, where all system noise and MTF effects are removed. The bar length-to-width ratio is 5:1. Because of the 3:4 aspect ratio of the sensor area, the Nyquist limit for vertical bars is 375 TV lines per picture height. The direct-view silicon sensor, with the high quantum efficiency of silicon, is the most sensitive sensor in the absence of system noise.

Case 2, shown in Figure 2, is again for 50% contrast vertical bars, but now includes system noise and MTF effects. RMS amplifier noise for the direct-view sensor is assumed to be 30 electrons per packet, while that for the EBS-CCD imagers is assumed to be 150 electrons. The EBS gain used is 2000, which is typically obtained in SIT tubes with V_{acc} of 10 keV. The proximity tube photocathode-to-target separation is 20 mils which is probably a lower limit for this parameter. No fixed pattern noise is included in this case. A detailed list of all other model parameter values used is given at the end of this section.

The EBS-CCD sensors outperform the direct-view CCD sensor at sensor irradiance levels below 6×10^{-6} W/m^2. Above this irradiance level, performance is roughly comparable for all sensors. The average sensor irradiance at which sensor-limiting resolution drops to 100 TVL/PH is about a factor of eight darker for the proximity tubes than for the direct-view CCD, and about a factor of 25 darker for the inverter tubes than for the direct-view CCD.

Case 3, shown in Figure 3, is a variation on Case 2 in which the gain of the EBS-CCD tubes has been reduced to 1000. The overall relationship of the curves to one another has not changed appreciably. The 100 TVL/PH limiting resolution point still occurs at a sensor irradiance level about a factor of 7 darker for the proximity tubes than for the direct-view CCD, and about a factor of 20 darker for the inverter tubes than for the direct-view CCD.

Case 4, shown in Figure 4, is another variation of Case 2, this one having fixed pattern noise included. The rms fixed pattern noise is assumed to be 30 electrons per pixel per field for the direct-view CCD, and 1000 electrons for the EBS-CCD tubes. All the curves have moved to higher irradiance

levels, but the EBS-CCD sensors still outperform the direct-view CCD. The 100 TVL/PH limiting resolution point occurs at an irradiance level about a factor of four times darker for the proximity tubes than for the direct-view CCD, and about 13 times darker for the inverter tubes than for the direct-view CCD.

Case 5, shown in Figure 5, is yet another variation on Case 2, in which the photocathode-to-target separation for the two proximity-focused tubes is increased to 50 mils. The curve for the GaAs proximity tube is essentially unchanged by this increase, while the curve for the S-20 proximity tube has dropped a little at the higher spatial frequencies. The reason for the different results is the wider angular distribution and higher emission energy for electrons emitted from the S-20 photocathode. Even for the S-20 proximity tube, however, the change is small, particularly at the lower light levels.

We now list the model parameter values not already given that have been used in the preceding analyses.

τ_f = 16 msec (sensor field time)

τ_{eye} = 0.1 sec (eye integration time)

α = 350 cm^{-1} (effective silicon optical absorption coefficient)

R = 0.3 (effective silicon optical reflectivity)

S = 1000 cm/sec (surface recombination velocity)

D = 35 cm^2/sec (minority carrier diffusion coefficient)

τ = 100 μsec (minority carrier lifetime)

L_n = 6 μm (thickness of neutral bulk layer)

L_s = 10 μm (total thickness of CCD substrate)

n_ϕ = 3 (number of phases)

ε_x = 10^{-5} (loss per transfer in output serial register)

ε_y = 10^{-5} (loss per transfer in sensor and storage registers)

J_D = 10 nA/cm^2 (dark current density in CCD at T = 300 K)

f_c = 7.8 MHz (output pixel clocking rate)

f_{co} = 150 ℓp/mm (lens cutoff frequency)

m_{pt} = 0.57 (photocathode-to-target minification for inverter tube)

f_σ = 35 ℓp/mm (one-sigma frequency for Gaussian pretarget MTF of inverter tubes)

V_{acc} = 10^4 V (accelerating voltage for proximity tubes)

E_e = {0.5 eV, for S-20 photocathodes, and 0.026 eV, for GaAs photocathode, (typical photoelectron emission energies for proximity tubes)

θ_e = {30°, for S-20 photocathode, and 7°, for GaAs photocathode, (typical photoelectron emission angles for proximity tubes).

C. SUMMARY

The low-light-level imaging performance of different EBS-CCD tubes has been analytically compared, along with that predicted for direct-view CCD imagers. Because its primary photosurface is silicon, the quantum efficiency of the direct-view CCD is higher than that of the EBS-CCD. However, since there is no gain prior to CCD readout, the noise-equivalent signal, referred to the CCD output, is considerably higher for the direct-view CCD, even when it is assumed that the noise is dominated by amplifier noise of a few tens of electrons per packet. For this assumption to be valid, the CCD must be cooled below room temperature in some fashion. Thus, in comparison with other forms of low-light-level image sensors, the EBS-CCD tube appears to offer significant advantages in terms of size, sensitivity, and temperature of operation.

II. STATUS OF ICCD DEVELOPMENT

A. INTRODUCTION

The development of charge coupled devices has had a major impact on all of the semiconductor industry. The self-scanning and direct read-out capabilities of these arrays eliminate the requirement of storage targets and read-out guns used in conventional camera tubes. The use of a CCD array incorporated into a vacuum tube envelope for operation in the electron bombarded mode utilizing a photocathode as the electron source will permit the advent of miniaturized

rugged, compact and simplified camera tubes and a new class of video processing devices for military and commercial applications.

The EOPD Tube and Sensor Laboratories at Fort Wayne, Texas Instruments, the Night Vision Laboratories at Fort Belvoir, and the NASA Goddard Space Center in Greenbelt have been working on the development of CCD devices for camera tube applications. Current development programs being carried out include the following.

- The development of a proximity focused diode tube incorporating a TI CCD array for operation in the electron bombarded mode.
- The development of a magnetically focused tube incorporating a TI CCD array for operation in the EB mode.

In addition, a general development program has been initiated within ITT to design and develop the necessary equipment to permit the monitoring of CCD electrical characteristics as a function of exposure to tube processing parameters and provide the means for the test and evaluation of the vacuum tubes being developed.

The following sections will briefly outline the primary objectives of the current programs, discuss the compatibility problems associated with subjecting a CCD array to the effects of vacuum tube processing, describe the two CCD tube designs being developed, and present results based on current data available.

B. PROGRAM OBJECTIVES

The primary objective of the current programs is to provide operational vacuum devices that will permit the test and evaluation of the performance characteristics of a charge coupled device, CCD, that is mounted in a vacuum tube envelope and operated in the electron bombarded mode. Two tube types are being developed, a proximity focused diode and a magnetically focused tube. Both tube types incorporate a TI 100 x 160 CCD array that has been mounted on a specially designed output flange.

The determination of the compatibility problems associated with subjecting a CCD array to the effects of vacuum tube processing as required for the development of CCD camera tubes is of prime importance. Specific compatibility problems under investigation include the following.

- The determination of the ability to incorporate a CCD header assembly into a vacuum tube envelope using standard heliarc welding procedures.
- Determination of the effects of vacuum baking during tube processing on the vacuum integrity of the CCD header assembly.
- Evaluation of the effects of vacuum baking on CCD electrical characteristics such as dark current and transfer efficiency.
- Evaluation of the effects of exposing the CCD array to alkali vapors required for photocathode formation.
- Determination of the performance characteristics of a CCD array operated in the electron bombarded mode.

C. PROXIMITY AND MAGNETIC FOCUS CCD TUBE DESIGNS

Both the proximity focused and the magnetic CCD tubes being developed consist of an all-metal-ceramic tube envelope, an output CCD header assembly, and magnesium fluoride input window. Both tubes are fabricated using ITT remote processing techniques wherein the photocathode is formed on the input window while physically isolated from the tube envelope in the vacuum forming chamber. Present contracts call for the use of a bialkali KCsSb cathode. After cathode formation, the input faceplate is transferred and indium sealed to the tube body. Both tube types use the same TI CCD header assembly, mounted on an ITT output flange. The CCD header assembly is shown in Figure 6.

An outline drawing of the ITT proximity ceramic envelope, the heliarc welded CCD header assembly and the re-entrant magnesium fluoride input window. The overall tube length is .60 inches. The tube has been designed to permit operation with 10-15 KV applied between the photocathode and the CCD array. The re-entrant cathode faceplate can be modified to accommodate changes in spacing required to achieve optimum resolution, consistent with acceptable field gradients and input energy levels required for optimum performance of the CCD array.

The magnetic tube design is shown in Figure 8. It consists of a brazed ceramic-metal stack that is 1.70 inches in diameter and approximately 3.6 inches in.length. The tube utilizes the same TI CCDheader assembly that is heliarc welded into the output section. .A gating mesh has been included and an indium sealed plano-plano magnesium fluoride input window completes the basic tube assembly. The tube is designed to operate at 20 KV and requires a 200 gauss magnetic field for first loop focus. The limiting resolution of the tube electron optics is in excess of one hundred line pairs per mm, exclusive of the CCD array characteristics.

An output photo of a potted ITT CCD diode is shown as Figure 9.

D. RESULTS TO DATE

To date, only tubes of the proximity focused design have been precessed, using available CCD header assemblies. It is expected that CCD header assemblies will be available in the near future to permit fabrication of the magnetic tubes.

Three TI CCD header assemblies were heliarc welded into ITT diode assemblies. The tubes were subjected to a 325°C vacuum bake, cathodes were remotely processed, transferred and sealed to the tube envelopes. All three tubes were shipped to NVL for test and evaluation. All tubes had TI arrays of the 100 x 160 buried channel design, mounted on a 33-pin header assembly and providing an active area of .08 cm^2 with a pixel dimension of 0.9 x 0.9 mils. All three tubes were checked for cathode stability for a minimum period of three weeks prior to shipment. No measurable change in cathode sensitivities was detected.

The first tube was operated in the EB mode at the NASA Goddard Space Center with the following preliminary results reported.

- The tube was operated with 12.5 KV applied between cathode and the CCD array.
- The array dark current from the active area was measured at 9 na, relative to an original measurement of 5.2 na measured prior to tube processing. This indicates less than a factor of two change in the total CCD dark current after being subjected to all tube processing parameters.
- An output resolution of 4 to 8 line pairs/mm was observed. Maximum resolution capability was not established. (The photocathode to CCD separation of .27 in. used would limit resolution to approximately 8 &p/mm.)
- Comparison of the output image quality with the CCD array operated in the EB mode to the image obtained with the array operated in the photoemissive mode showed no essential difference, with the exception of a somewhat higher granular appearance of the EB output.

It should be noted that the first tube processed and described above did not contain a re-entrant cathode faceplate, and therefore, did not provide optimum cathode to CCD array spacing. The array dark current on the second and third tubes delivered indicated an increase by a factor of three and ten relative to original measurements prior to processing. In addition, preliminary tests on these two tubes have indicated the presence of an inoperable sector within the 100 x 160 CCD arrays. The nature and cause of these conditions is currently under further investigation.

Although the above data is preliminary, and indeed limited in detail and scope, it does permit the following observations to be made.

- TI CCD header assemblies can and have been subjected to heliarc welding, vacuum bake, and tube processing cycles without loss of vacuum integrity.
- Tube processing and cathode formation had no known adverse effects on the electrical characteristics of the CCD array. Dark current on the first array remained within a factor of two of original levels.
- Output imagery has been achieved from a TI CCD array sealed into a miniaturized ITT diode structure and operated in the electron bombarded mode.

Additional data and information will become available as programs similar to those discussed herein proceed beyond their first year of implementation.

ACKNOWLEDGEMENTS

We hereby wish to acknowledge the technical efforts and contributions of Mr. Donald H. Ceckowski, CCD Project Engineer, EOPD, Fort Wayne, and the support of Mr. Andrew Kennedy, CCD COTR, NVL, and Mr. Jack Williams, CCD COTR, NASA/Goddard.

REFERENCES

1. F. A. Rosell and R. H. Willson, "Performance Synthesis (Electro-Optical Sensors)," Westinghouse Defense and Electronic Systems Technical Report, AFAL-TR-72-279 (August 1972); _____, "Performance Synthesis of Electro-Optical Sensors," Westinghouse Defense and Electronic Systems Technical Report, AFAL-TR-73-260 (August 1973); _____, "Performance Synthesis of Electro-Optical Sensors," Westinghouse Defense and Electronic Systems Technical Report, AFAL-TR-74-104 (April 1974).

2. J. B. Barton, "Development of Electron-Bombarded Silicon (EBS) Charge Coupled Device (CCD) Imagers," Final Technical Report by Texas Instruments Incorporated on NVL Contract No. DAAK02-74-C-0359 (May 1975), pp. 43-96.

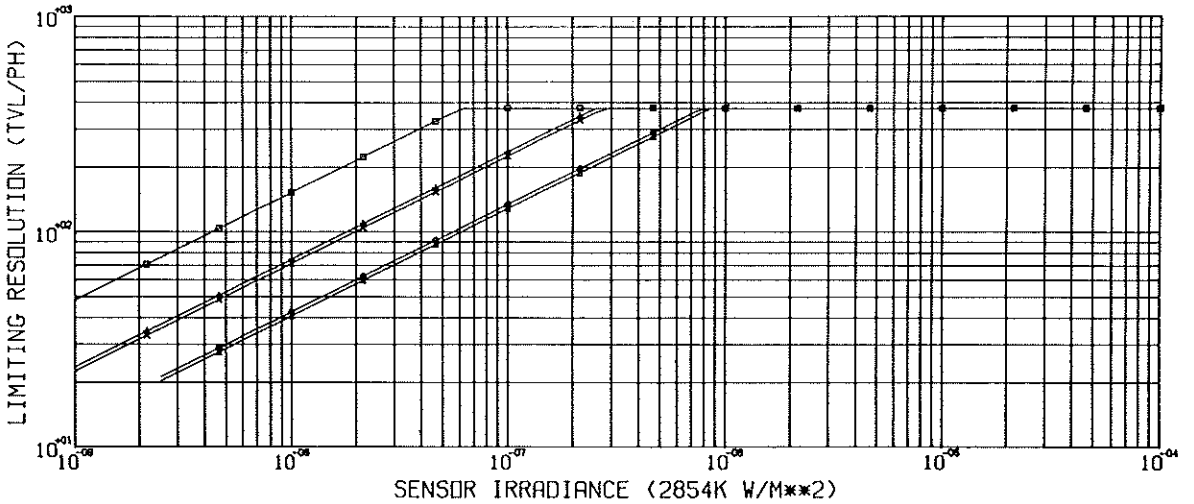

□ Direct-View CCD
○ Proximity-Focused EBS-CCD, S-20 Photocathode
△ Proximity-Focused EBS-CCD, GaAs Photocathode
\+ Inverter EBS-CCD, 25 mm S-20 Photocathode
X Inverter EBS-CCD, 25 mm GaAs Photocathode

Case 1. Photon-Noise-Limited Resolution of 500 x 500 Imagers; No MTF Effects Included; Vertical Bars in Test Pattern

FIGURE 1

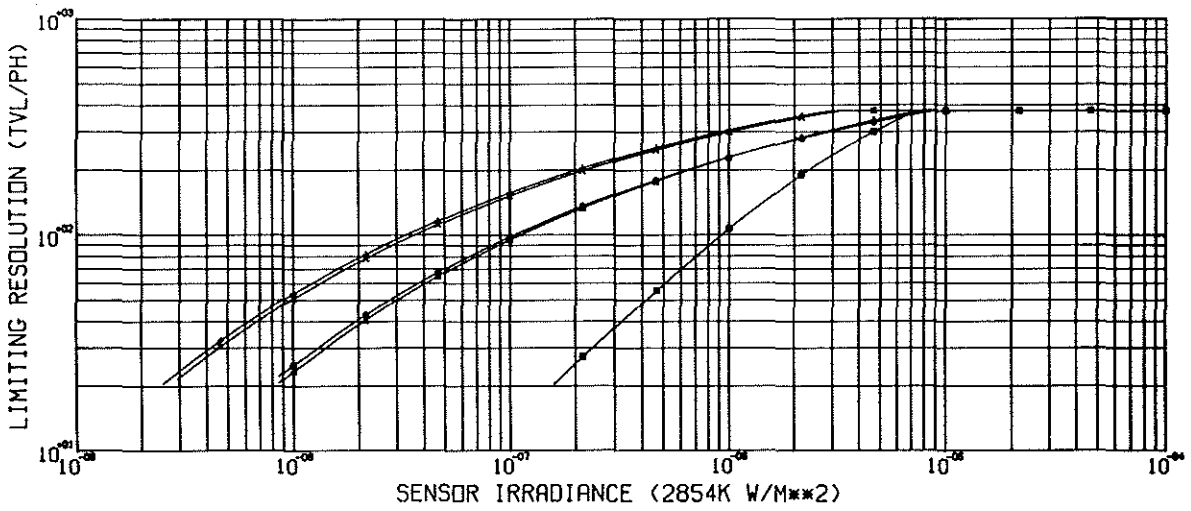

□ Direct-View CCD, T = 210 K, N_{na} = 30 Electrons
○ Proximity-Focused EBS-CCD, S-20 Photocathode
△ Proximity-Focused EBS-CCD, GaAs Photocathode
\+ Inverter EBS-CCD, 25 mm S-20 Photocathode
X Inverter EBS-CCD, 25 mm GaAs Photocathode

} T = 300 K, N_{na} = 150 Electrons

Case 2. Limiting Resolution with System Noise and MTF Effects Included; Vertical Bars in Test Pattern

FIGURE 2

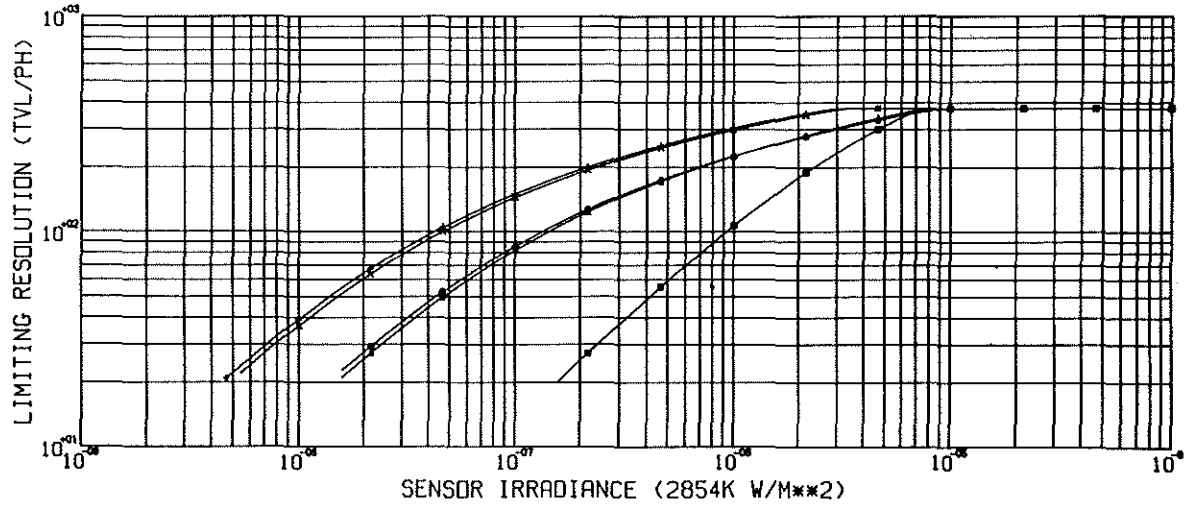

□ Direct-View CCD, T = 210 K, N_{na} = 30 Electrons
○ Proximity-Focused EBS-CCD, S-20 Photocathode
△ Proximity-Focused EBS-CCD, GaAs Photocathode
\+ Inverter EBS-CCD, 25 mm S-20 Photocathode
X Inverter EBS-CCD, 25 mm GaAs Photocathode

} T = 300 K, N_{na} = 150 Electrons

Case 3. Variation on Case 2, with EBS-CCD Gain Reduced to 1000

FIGURE 3

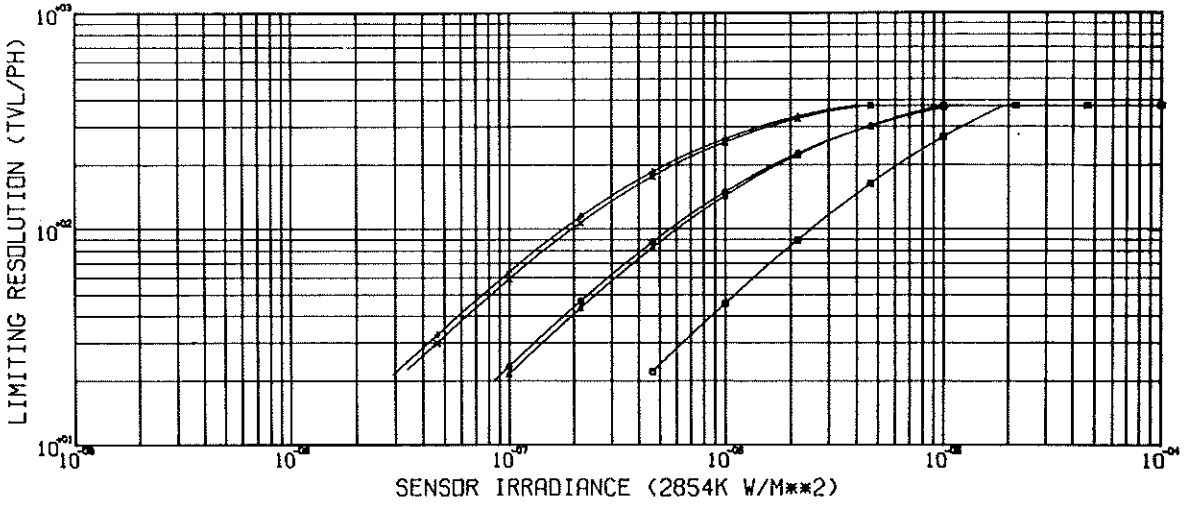

□ Direct-View CCD, T = 210 K, N_{na} = 30 Electrons
○ Proximity-Focused EBS-CCD, S-20 Photocathode
△ Proximity-Focused EBS-CCD, GaAs Photocathode
\+ Inverter EBS-CCD, 25 mm S-20 Photocathode
X Inverter EBS-CCD, 25 mm GaAs Photocathode

} T = 300 K, N_{na} = 150 Electrons

Case 4. Variation on Case 2, with Fixed Pattern Noise Included

FIGURE 4

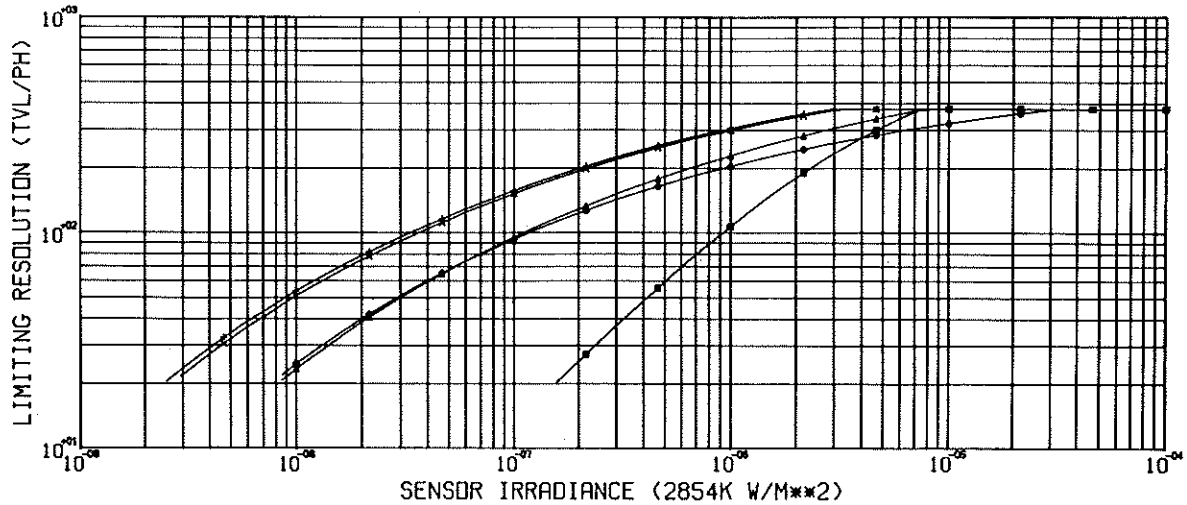

□ Direct-View CCD, T = 210 K, N_{na} = 30 Electrons
○ Proximity-Focused EBS-CCD, S-20 Photocathode
△ Proximity-Focused EBS-CCD, GaAs Photocathode
\+ Inverter EBS-CCD, 25 mm S-20 Photocathode
X Inverter EBS-CCD, 25 mm GaAs Photocathode

} T = 300 K, N_{na} = 150 Electrons

Case 5. Variation on Case 2, with Proximity Tube Photocathode-to-Target Separation Increased to 50 Mils

FIGURE 5

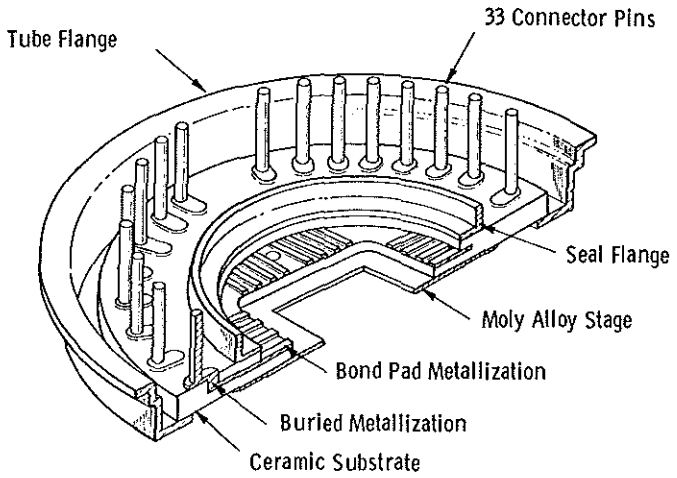

TI CCD Header Assembly

FIGURE 6

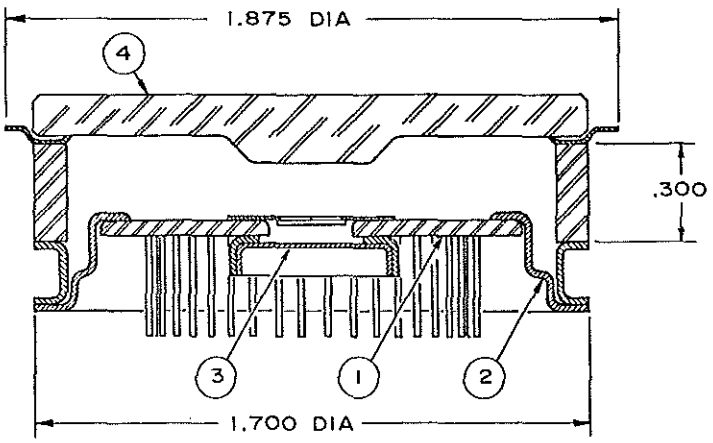

ALL DIMENSIONS ARE IN INCHES

(1) CCD-HEADER
(2) MOUNTING FLANGE FOR CCD HEADER
(3) NIROMET CAP
(4) MAGNESIUM FLUORIDE OR DYNASIL UV1000 FUSED SILICA INPUT WINDOW

ITT Proximity Focused CCD Diode

FIGURE 7

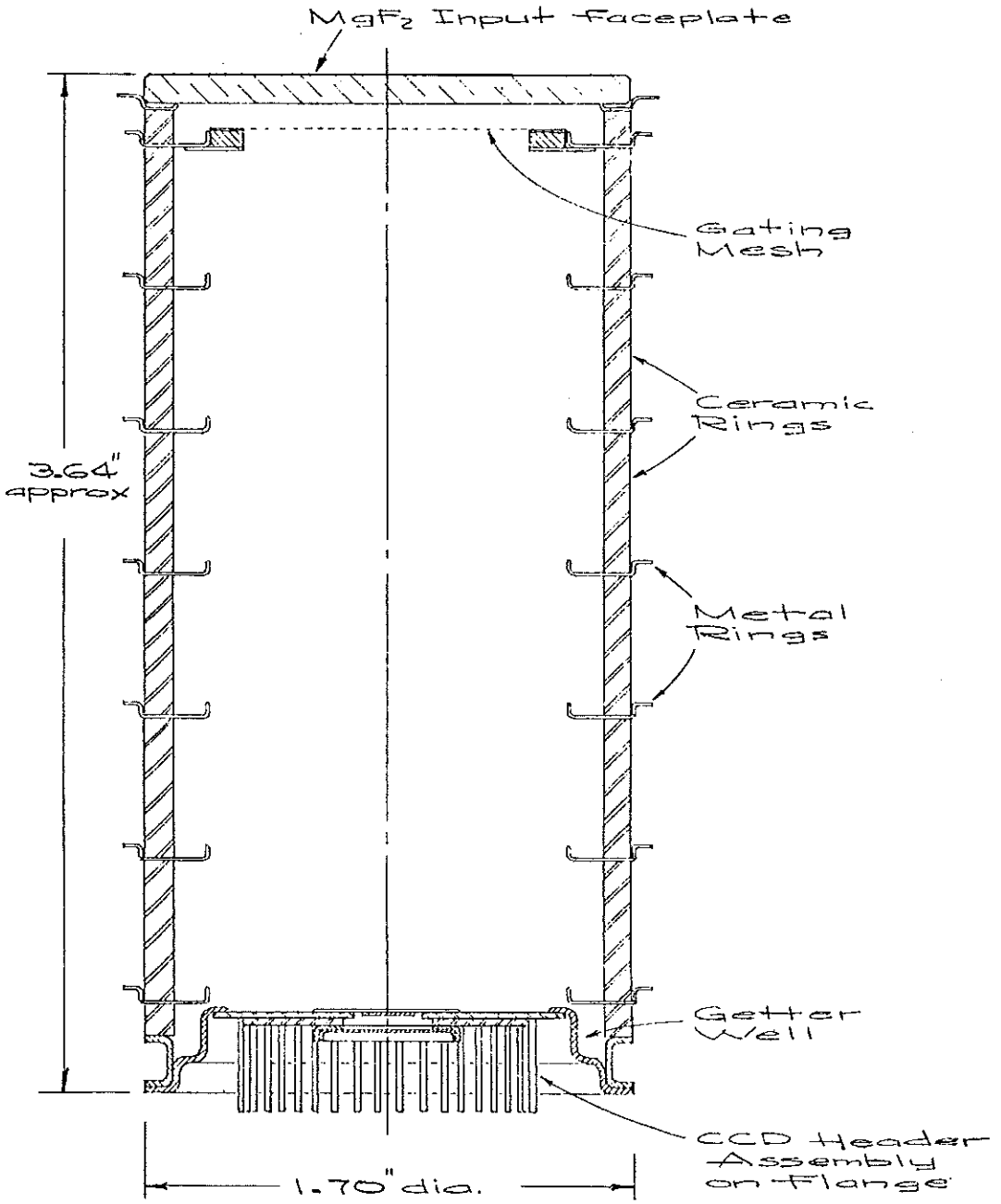

Magnetic Focus ICCD

FIGURE 8

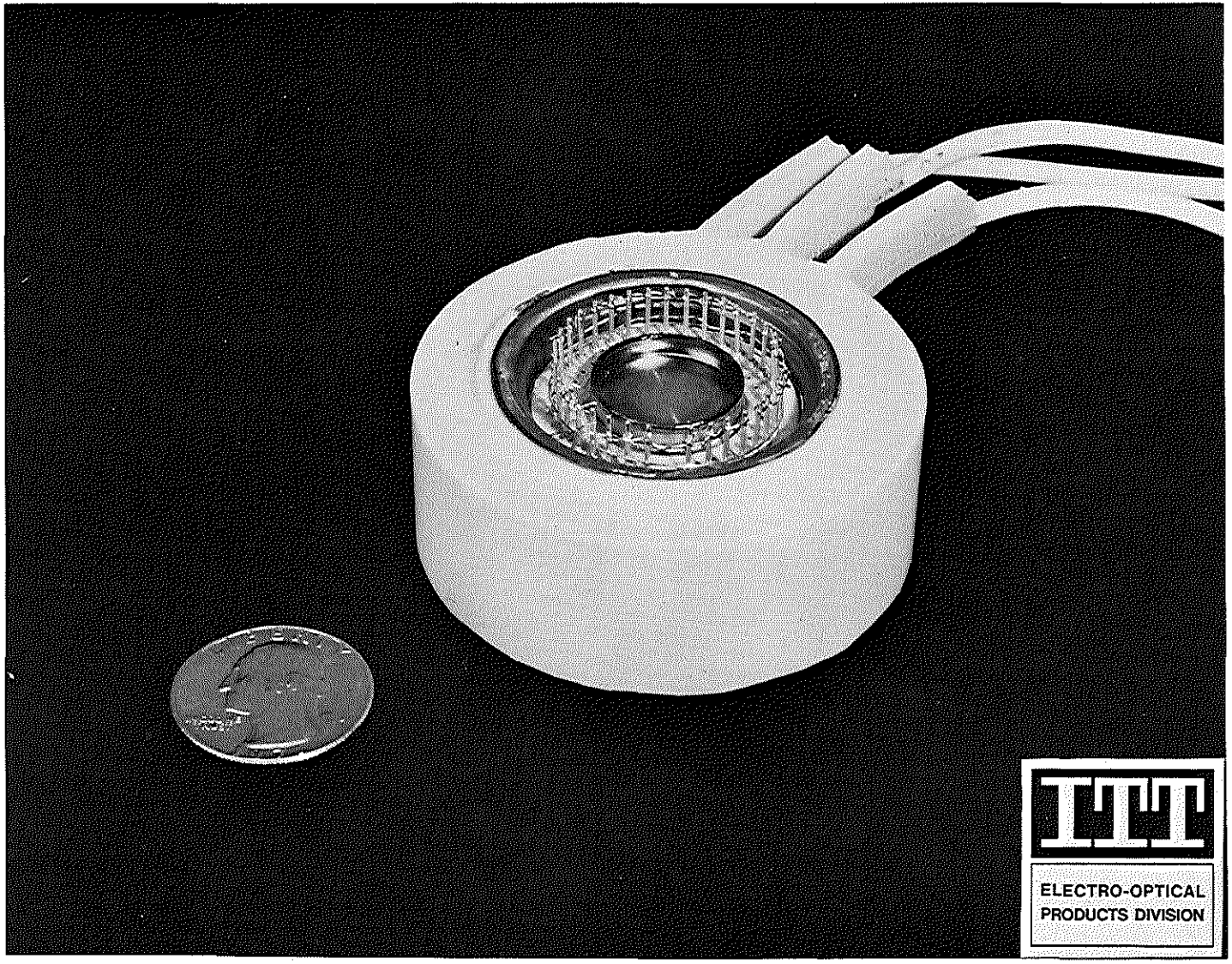

FIGURE 9. Potted CCD Diode